

Supplementary information

Electrochemical decarboxylation of acetic acid on boron-doped diamond and platinum functionalised electrodes for pyrolysis-oil treatment

Talal Ashraf^a, Ainoa Paradelo Rodriguez^a, Bastian Timo Mei^{*a,b}, Guido Mul^a

^aPhotoCatalytic Synthesis Group (PCS-TNW), University of Twente, Enschede, The Netherlands; ^bIndustrial Chemistry, Ruhr-Universität Bochum, Bochum, Germany.

1. Reaction mechanism of Kolbe/Hofer Moest reaction of acetic acid

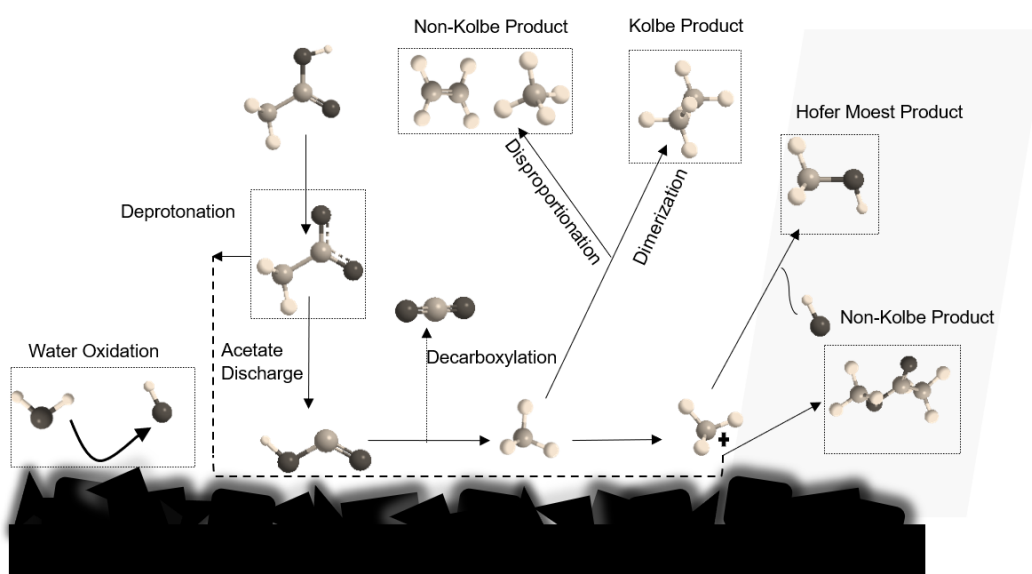


Figure S1: (non) Kolbe electrolysis reaction mechanism of acetic acid on platinum electrodes based on literature ^{1,2}.

2. Schematic representation of divided flow cell with continuous flow and inline gas analysis

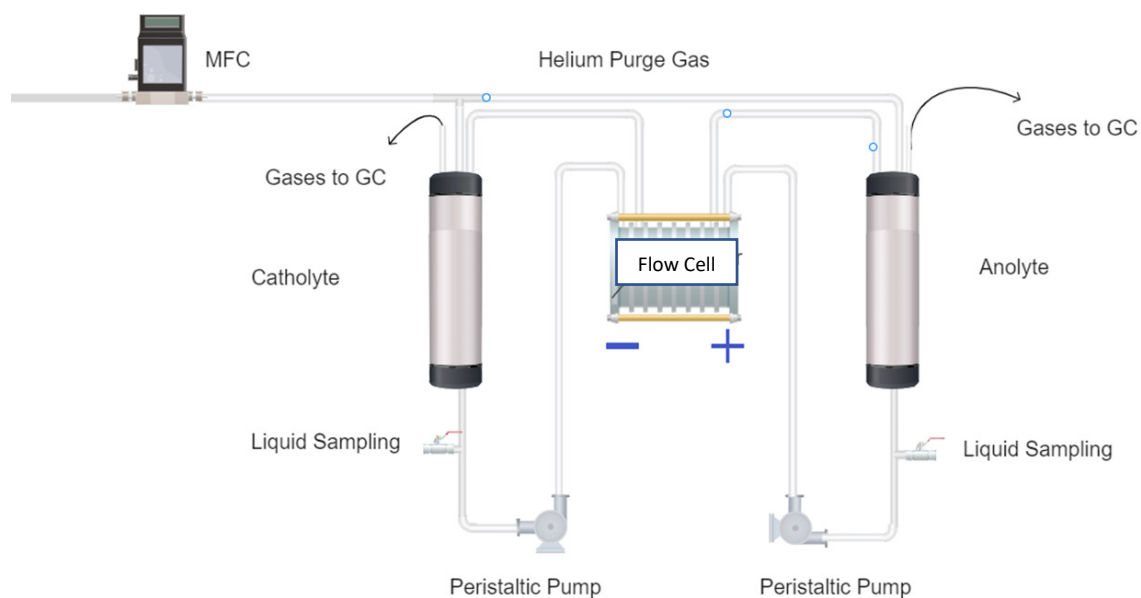


Figure S2: Schematic representation of flow cell with different catholyte and anolyte compartments with insitu facility of gas analysis during the reaction. Liquid samples are collected at the end of experiment from sampling port.

3. Faradaic efficiency w.r.t for different electrodes (BDD, Graphite, FTO, Nickel Foam)

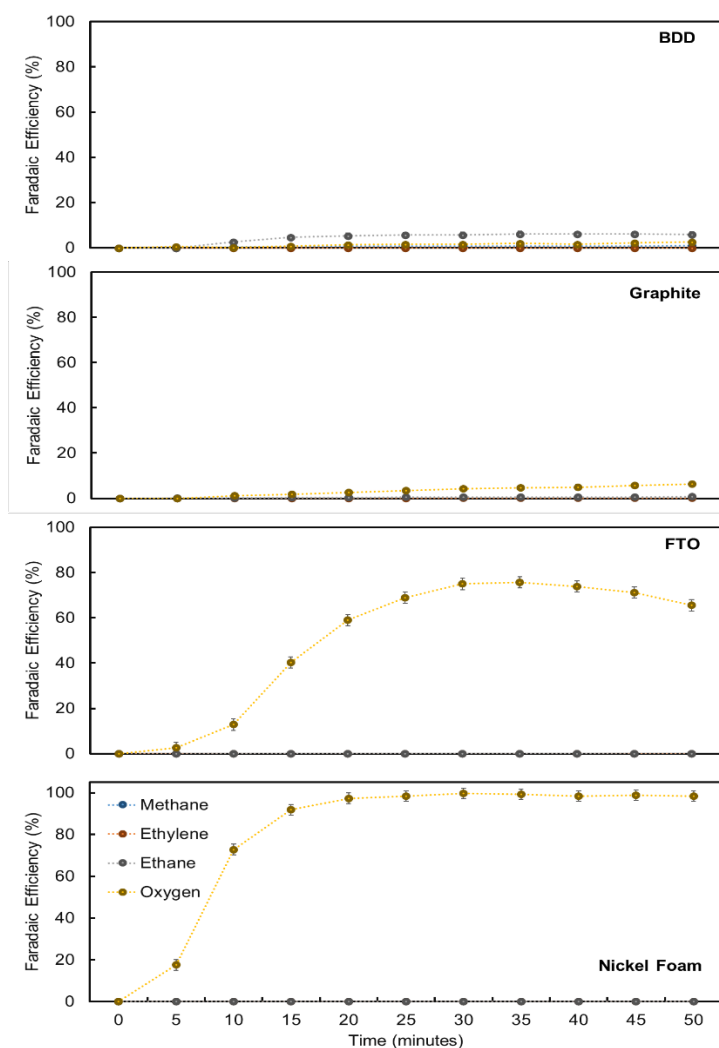


Figure S3: Faradaic efficiency within timeframe during the electrolysis of 1M Na-acetate/acetic acid pH5 at 25 mA/cm² on different bare substrates (BDD, Ni foam, FTO and Graphite).

4. Electrolysis of acetic acid at constant current on different electrodes

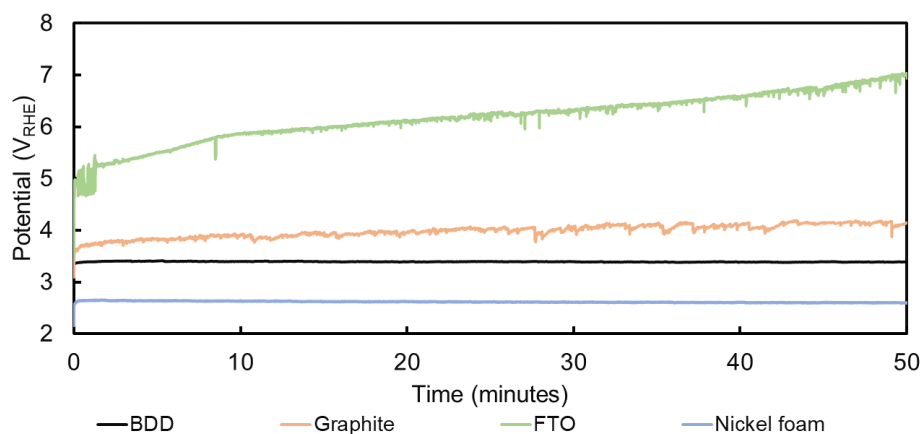


Figure S4: Chronopotentiometry and working electrode potential within the electrolysis time of 50 minutes for different bare electrodes during electrolysis at 25mA/cm² in 1M acetic acid/Na-acetate, solution pH5.

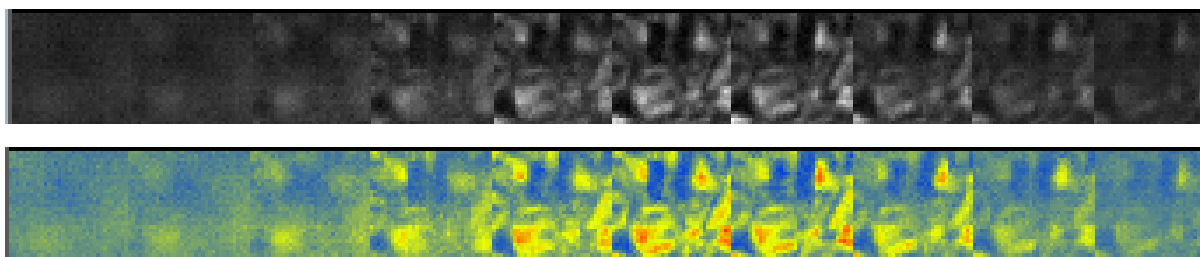
5. Raman spectroscopy of BDD electrodes

Since the surface is very rough (a few μm 's) the signal intensity depends a lot on the chosen depth when recording a confocal image or spectral data from such a layer.

Therefore a z-stack of images is taken to determine the optimal depth, Z-image stack (10) of BDD sample (unused). The distance in Z between the images are 1 μm

- The scanned area is 10x10 μm at 40x40 raster
- Measurement conditions: 35mW, 150ms, Gain4, 50KHz, Obj: Olymp40xNA0.95

Diamond band:



Boron band:

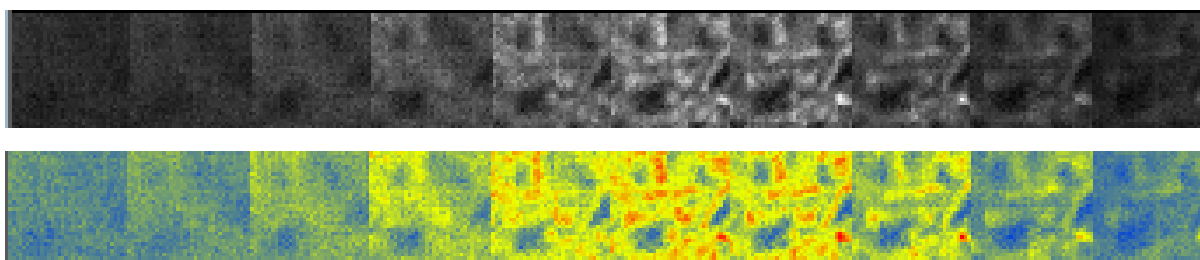


Figure S5: Z stack images of the BDD electrode within the depth from the top of the surface, captured by confocal microscope with Raman spectrometer. Contrast showing the signal intensity of boron and diamond bands.

6. SEM Image of BDD before and after electrolysis of acetic acid at 25mA/cm²

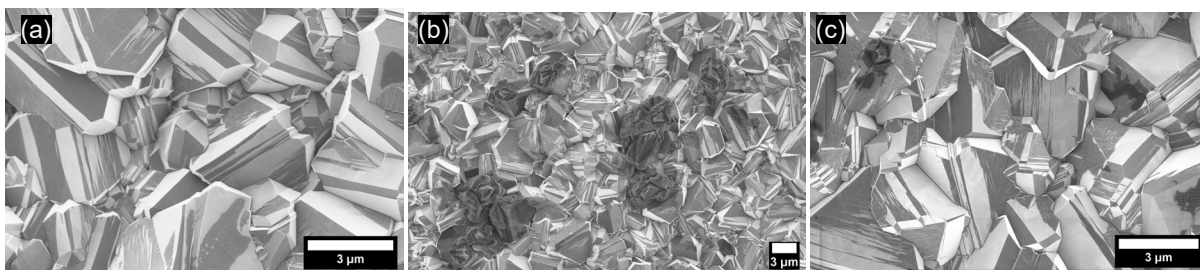


Figure S6: SEM analysis of bare BDD in 1M acetic acid/sodium acetate pH 5 at 25 mA/cm² (a) before oxidation, (b) after oxidation-graphitised carbon visible, (c) after cleaning.

From these results about 3 images contain the highest signal and also contrast. When we select the 3 best images out of a stack, we will ensure that the measurement is done on the same depth inside the layer of a sample. This will allow us to compare spectra of different samples.

7. Effect of acetic acid concentration on the product distribution of acetic acid electrolysis on BDD

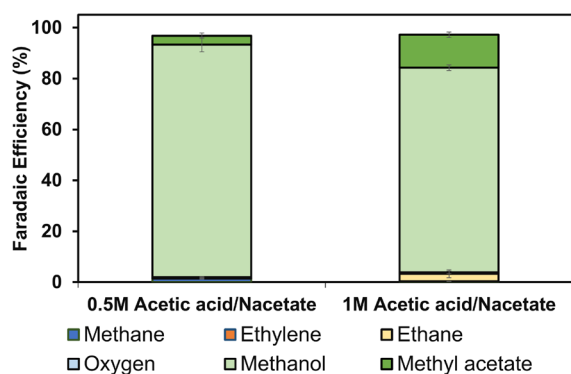


Figure S7: Effect of acetic acid/sodium acetate concentration (pH 5) on electrooxidation on BDD electrode at 50 mA/cm² and 60 ml/min in flow cell.

8. ECSA and CV of platinum sputtered layer with different thickness on BDD electrodes

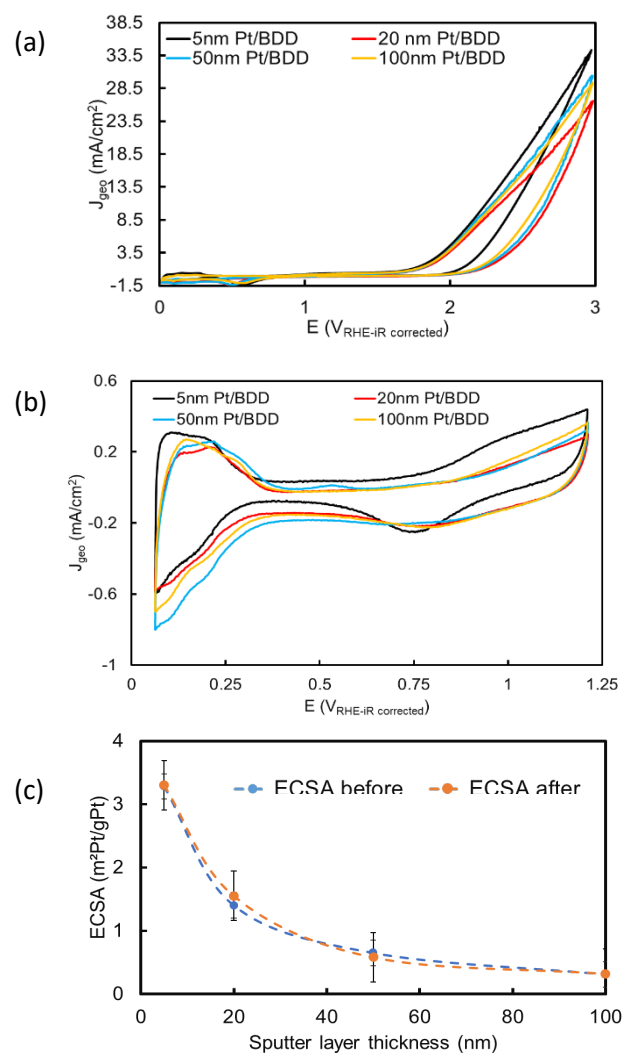


Figure S8: (a) Cyclic voltammogram of 5, 20, 50 and 100 nm sputtered thin film of platinum on the BDD surface in 1M acetic acid/Na-acetate solution pH5 (b) CVs in the range 0.05-1.2V_{RHE} for determination of ECSA in 1M H₂SO₄. (c) ECSA

9. ECSA and roughness factor of platinum sputtered layer with different thickness on BDD electrodes

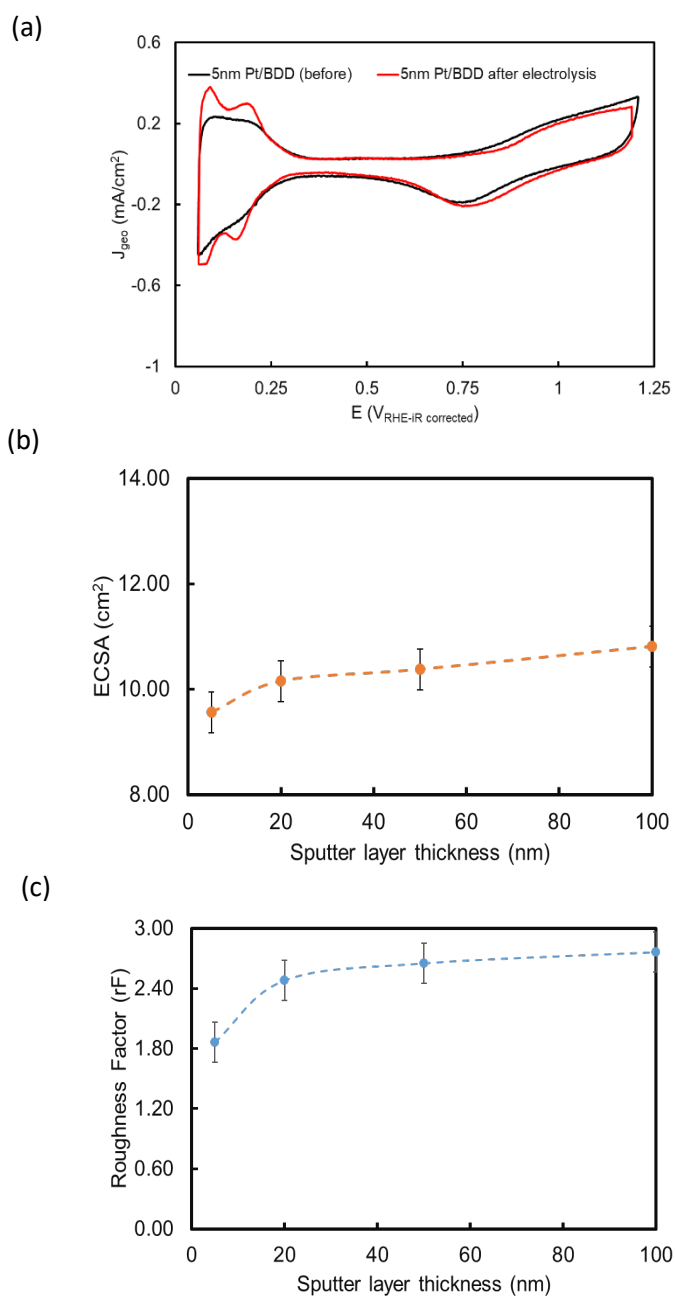


Figure S9: (a) CV of 5nm sputter cycle before and after electrolysis of acetic acid/sodium acetate for 1 M acetate solution. (b) ECSA relationship with the platinum sputter layer thickness (c) The correlation of roughness factor

10. Faradaic efficiency w.r.t time frame of 100 mins on 5nm Pt/BDD electrode

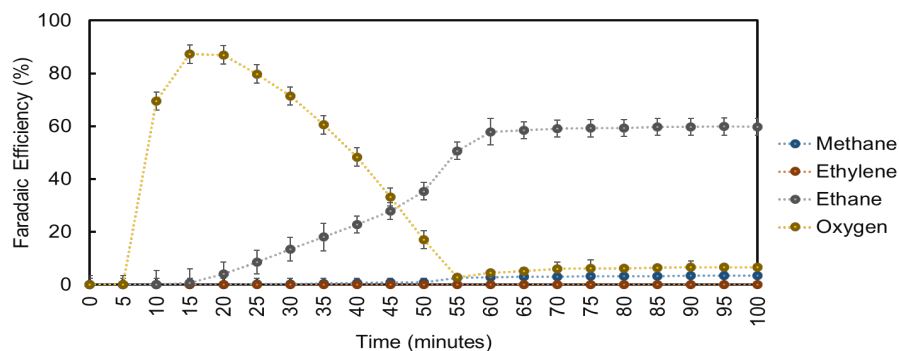


Figure S 10: The faradaic efficiency in extended time scale of 5nm thin platinum layer showing the transition of OER to Kolbe in 1M acetic acid/sodium acetate pH 5 at 25

11. Faradaic efficiency w.r.t time frame of 50mins on different sputter Pt/BDD electrode layer thickness

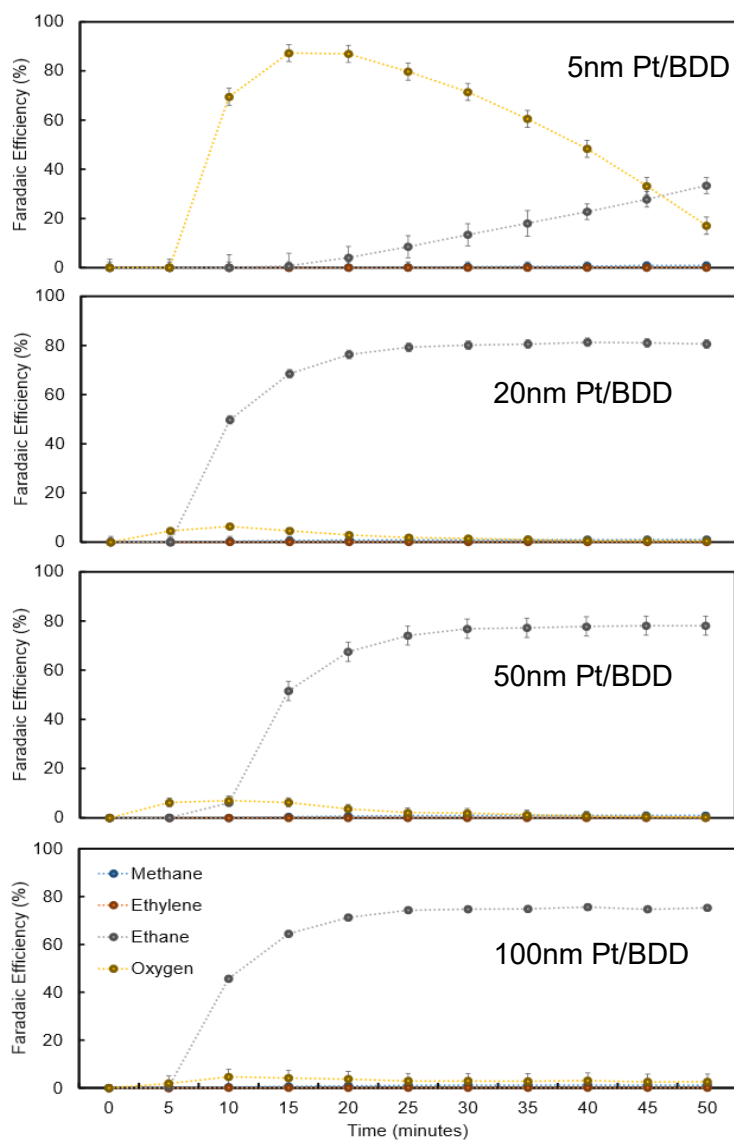


Figure S11: Faraday efficiency in time scale during electrolysis for methane, ethylene, ethane, and oxygen on 5, 20, 50 and 100 nm thin platinum layer on BDD in 1M acetic acid/Na acetate pH 5 at 25 mA/cm²

12. Faradaic efficiency w.r.t time frame of 50mins on Platinum foil electrode

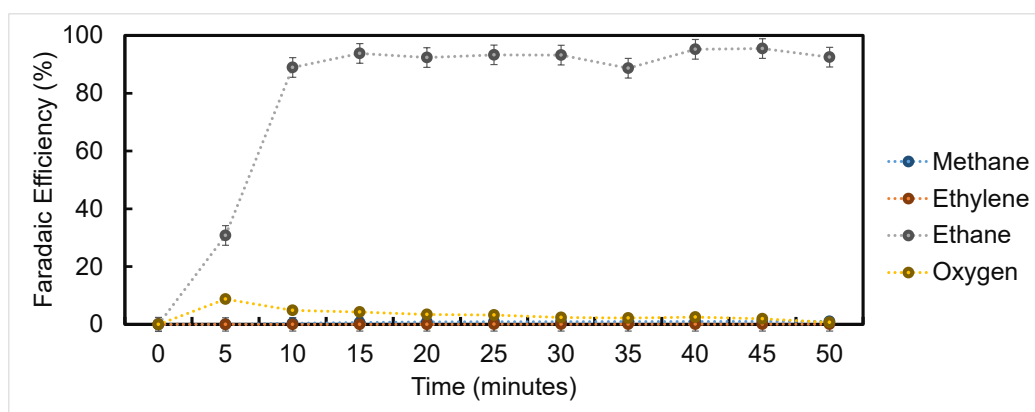


Figure S 12: The faradaic efficiency in extended time scale of Kolbe electrolysis on Pt foil in 1M acetic acid/sodium acetate pH 5 at 25 mA/cm²

13. SEM image of acetate coverage on 5nm platinum sputtered layer on BDD

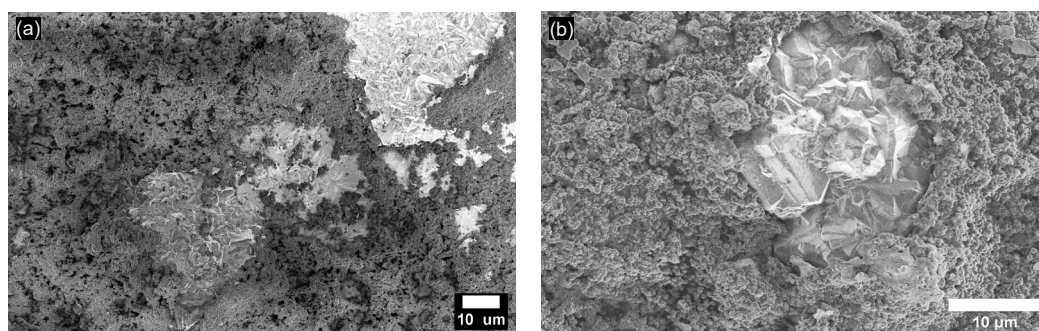


Figure S13: Acetate coverage on 5nm thin platinum layer on BDD after 1Hr electrolysis of 1M Na-acetate/acetic acid at pH5 and 25mA/cm² in three electrode batch cell reactor.

14. Production rate of (non) Kolbe/Indirect oxidation products on platinum sputtered electrodes

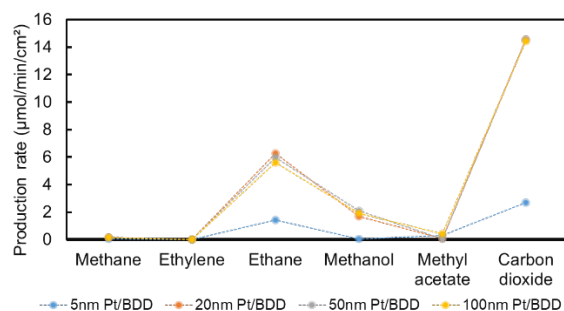


Figure S14: Production rate of (non)Kolbe and indirect oxidation product on thick layers (5, 20, 50,100nm) of platinum on BDD in 1M acetic acid/sodium acetate pH 5 at 25 mA/cm².

15. CV of electrodeposited platinum nanoparticles (nanoflowers, mono dispersed nanoparticles, nano thorns, and nanocrystals) in H₂SO₄ and acetic acid/sodium acetate

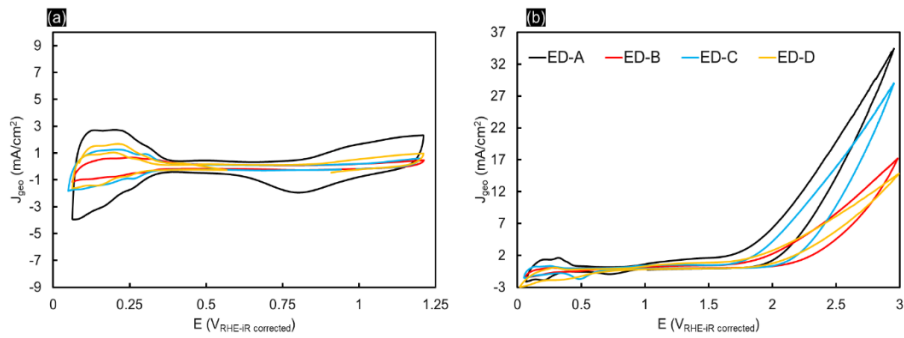


Figure S15: (a) CV of electrodeposited platinum nanoparticles in 1M H₂SO₄ for ECSA determination (b) CV of electrodeposited platinum nanoparticles in 1M acetic acid/sodium acetate.

16. Correlation of platinum nanoparticles loading with ECSA(cm²)

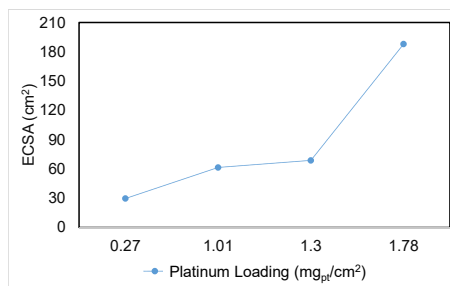


Figure S16: The ECSA in correlation with the platinum loading showing that ECSA increases with the platinum content.

17. Faradaic efficiency w.r.t time frame of 50mins on different platinum nanoparticles geometry

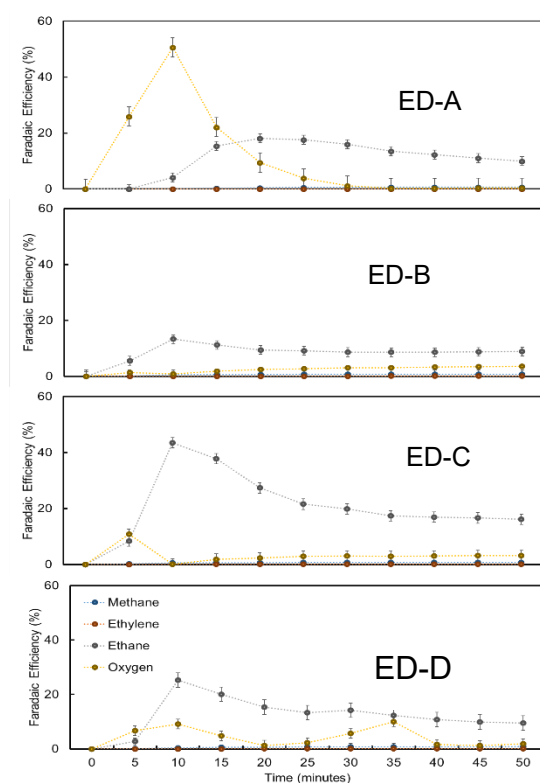


Figure S17: Faradaic efficiency within time during the electrolysis of 1M Na-acetate/acetic acid pH 5 at 25 mA/cm² on different shape platinum nanoparticles (nanoflowers ED-A, homogeneously dispersed nanoparticles ED-B, nano thorns ED-C, nanocrystals ED-D).

18. SEM image of platinum nanoflower deposition for 30 mins before and after electrolysis

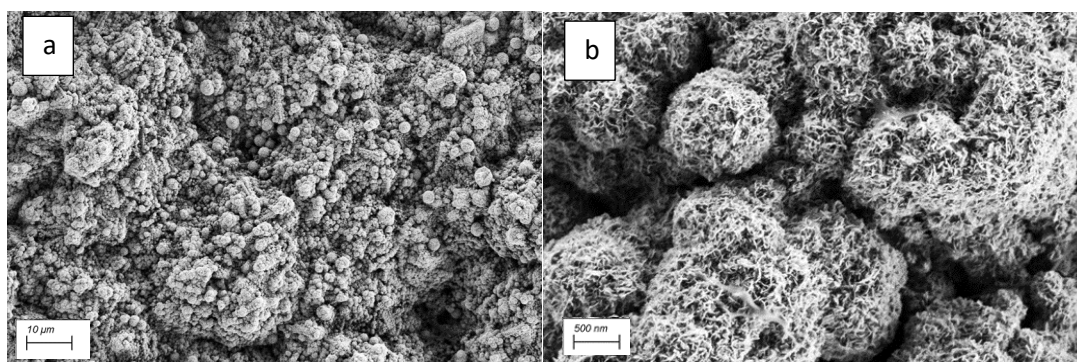


Figure S18: (a)ED-A deposition after 30 minutes on BDD (b) ED-A after electrolysis in 1M Acetic acid/Na-acetate pH 5 at 25 mA/cm².

19. Faradaic efficiency towards (non) Kolbe/indirect oxidation products w.r.t electrodeposition time of platinum nanoflowers

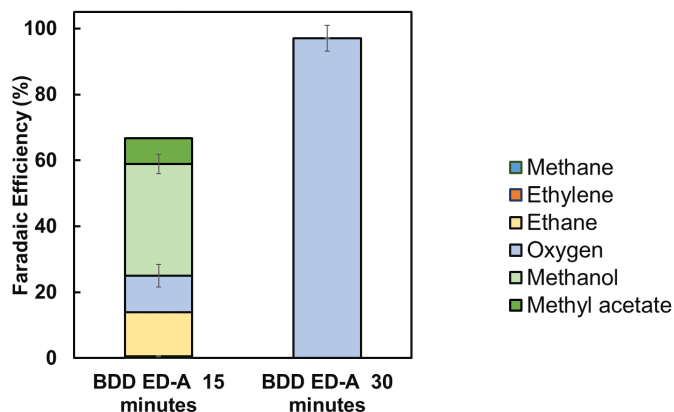


Figure S19: Faradaic efficiency of BDD with ED-A nanoflowers platinum deposition method with different time (15, 30 minutes) in 1M acetic acid/sodium acetate pH 5 at 25 mA/cm².

20. EDS image of platinum nanoparticles deposited on the Nickel foam confirming the presence of platinum content

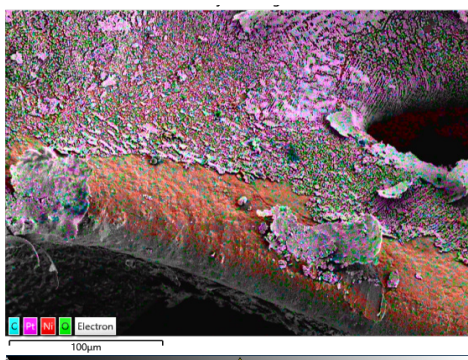


Figure S20: EDS image of platinum nanoparticles deposited on the Nickel foam, confirming the presence of platinum by ED-A deposition method.

21. Chronopotentiometry during electrooxidation of acetic acid at 25mA/cm² on sputtered platinum layers on BDD

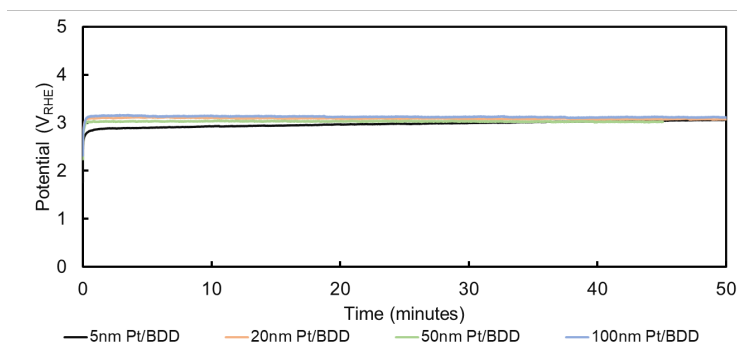


Figure S21: Chronopotentiometry working electrode potential within the electrolysis time scale for sputter layers of platinum with different thickness on BDD in 1M acetic acid/sodium acetate pH 5 at 25 mA/cm².

22. Production rate of (non) Kolbe/Indirect oxidation products on different electrodes

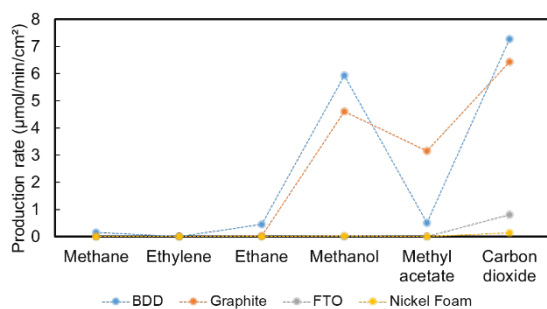


Figure S22: Production rate of Kolbe and indirect oxidation product on bare electrodes in 1M acetic acid/sodium acetate pH 5 at 25 mA/cm².

23. Chronopotentiometry during electrooxidation of acetic acid at 25mA/cm² on platinum nanoparticles on BDD

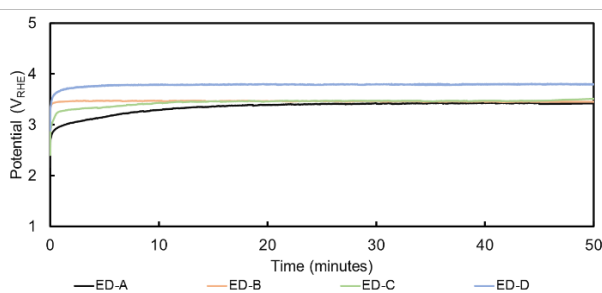


Figure S23: Chronopotentiometry working electrode potential within the electrolysis time scale for nanoparticles on BDD electrodes during electrolysis at 25mA/cm² in 1M acetic acid/Na-acetate solution pH5.

24. Production rate of (non) Kolbe/Indirect oxidation products on platinum nanoparticles on different substrates

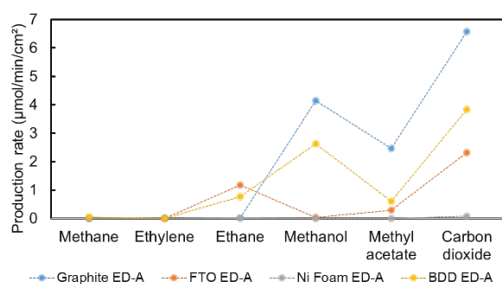


Figure S24: Production rate of Kolbe and indirect oxidation product of nanoflowers ED-A deposited nanoparticles on different substrate electrodes.

25. Faradaic efficiency w.r.t time frame of 50mins on platinum nanoflowers on different substrates

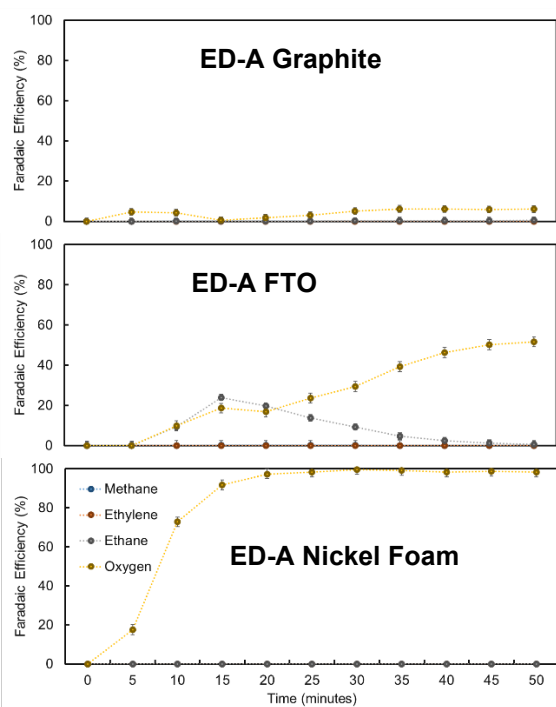


Figure S25: Faradaic efficiency within time during the electrolysis of 1M Na-acetate/acetic acid pH 5 at 25 mA/cm² on different substrates with nanoflowers ED-A nanoparticles for 50 minutes.

26. Faradaic efficiency w.r.t time frame of 60 minutes on BDD during continuous flow electrolysis at 50mA/cm² at different pH

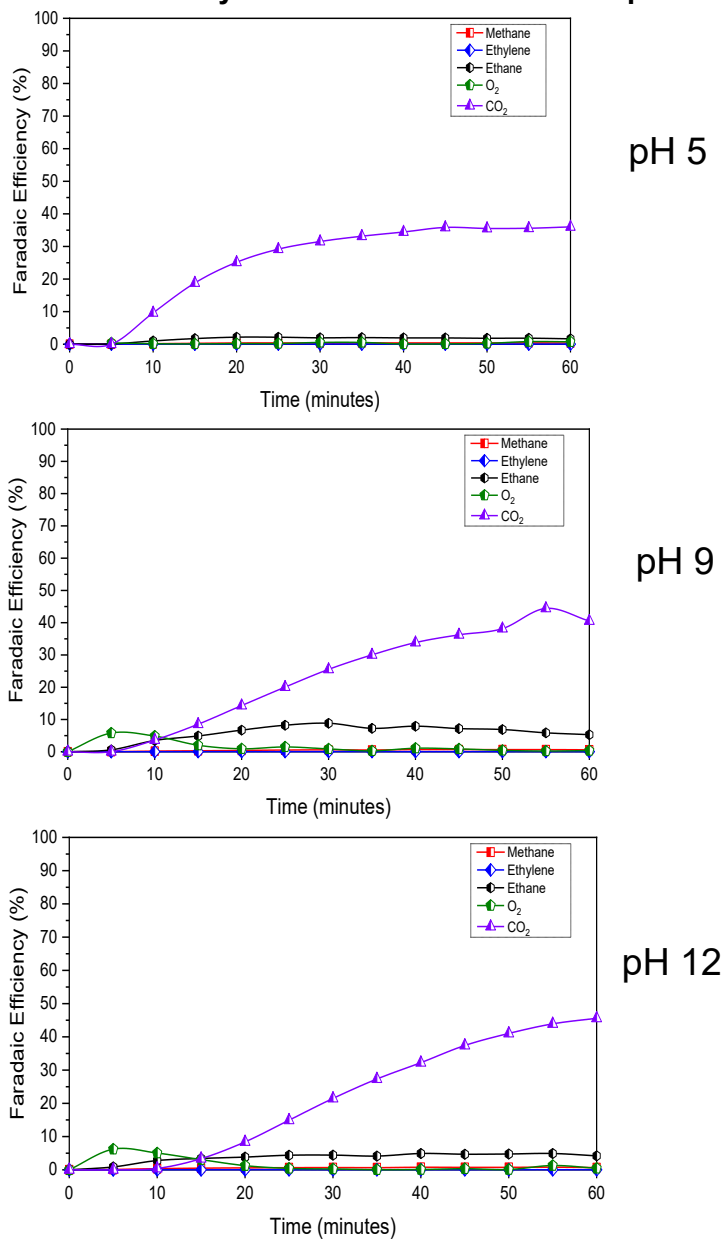


Figure S26: pH Impact on electrooxidation of 1M acetic acid/ sodium acetate at 50 mA/cm² and pH 5,9,12 on BDD electrode in flow cell with continuous electrolyte recirculation rate of 60ml/min.

27. Comparison of EC-MS And DEMS technology

There are many differences in ECMS and DEMS: ECMS is the latest commercial technology compared to DEMS, which is more often homemade; ECMS is advantageous in terms of sensitivity, reproducibility, electrolyte saturation, time resolution and time resolution and quantification and dynamic range. ECMS provides high turnover resolution for gaseous analytes with 100% collection efficiency and fast control of dissolved gases. ECMS membrane chips are precisely made by accurate and high-quality microfabrication providing high reproducibility due to a well-defined flux of molecules. Porous Teflon DEMS membranes are naturally highly variable in their characteristics. DEMS runs in flow mode, which can cause the reaction products to be lost in flow conditions; the water evaporation rate in DEMS is higher. It is impossible to measure the small number of products with decent time resolution with DEMS ECMS cells operating in a stagnant cell without differential pumping. It is also possible to quantify the sub-monolayer concentrations. More information is available at ([DEMS Comparison - Spectro Inlets](#)).

References

1. S. Liu, N. Govindarajan, H. Prats and K. Chan, *Chem Catal.*, 2022, **2**, 1100–1113
2. N. Kurig, J. Meyers, F. J. Holzhäuser, S. Palkovits and R. Palkovits, *ACS Sustain. Chem. Eng.*, 2021, **9**, 1229–1234.